IEEE Access
Multidisciplinary ⋮ Rapid Review ⋮ Open Access Journal

Received April 28, 2022, accepted May 12, 2022, date of publication May 16, 2022, date of current version May 26, 2022.

Digital Object Identifier 10.1109/ACCESS.2022.3175501

An Improved Model Free Predictive Current Control for PMSM With Current Prediction Error Variations

PENG WANG[1], XIN YUAN[2], (Member, IEEE), AND CHENGNING ZHANG[1]
[1]National Engineering Laboratory for Electric Vehicles, School of Mechanical Engineering, Beijing Institute of Technology, Beijing 100081, China
[2]School of Electrical and Electronic Engineering, Nanyang Technological University, Singapore 639798

Corresponding author: Chengning Zhang (zhang_cn123@163.com)

This work was supported in part by the Key Areas of Guangdong Province through the Project "Integration and Industrialization of High Performance, Long Endurance, and Integrated Electric Drive System" under Grant 2019B090910001.

ABSTRACT The conventional model predictive current control is a model-based control method, and the accuracy of the predicted currents is affected by motor parameters such as flux linkage, inductance, and resistance. To get rid of model parameters dependencies, a model-free predictive current control (MFCC) was proposed before, which can improve the parameter robustness without utilizing any knowledge of the initial motor parameters. However, the stagnant current update detection is one of the main problems that limit the current predictive performance. To solve this problem, a current prediction error model according to the contiguous instant current error variations is proposed to reconstruct the surface-permanent magnet synchronous motor (SPMSM) model in this paper. Afterwards, a novel MFCC method with the online parameter identification is developed. This method takes advantage of mathematical relationships in the current prediction error model, and the motor parameters can be updated within each period to improve prediction accuracy. Simulation and experimental results verify that this proposed MFCC method can significantly reduce the stagnation effect and improve MFCC performance under different parameter disturbances.

INDEX TERMS Model-free predictive current control (MFCC), parameter robustness, surface-permanent magnet synchronous motor (SPMSM).

I. INTRODUCTION

Recently, model predictive control (MPC) has received extensive attention in electric drive applications due to its clear concept, fast dynamic response, and simple implementation [1]. The principle of MPC is to predict the expected behavior in a future time window by minimizing a cost function.

A. LITERATURE REVIEW

Generally, there are two main types of MPC. The continuous control set MPC (CCS-MPC) is the first type, which uses the space vector pulse modulation (SVPWM) to generate infinite voltage vectors [2]. By contrast, the finite control set MPC (FCS-MPC) is another type, which makes full use of the discrete characteristics of the inverter to output a limited number of switching state [3], [4].

The associate editor coordinating the review of this manuscript and approving it for publication was Alfeu J. Sguarezi Filho.

In the previous work [5], FCS-MPC can also be classified into two types. The model predictive torque control (MPTC) is the first type, in which the weight factor is an important parameter to be considered, and the improper selection will lead to the system performance degradation [6]. The model predictive current control (MPCC) is another type. Compared with MPTC, the MPCC contains only the current prediction errors in the cost function, which effectively eliminates the weight factor and reduces the control complexity [7]–[9]. In this case, MPCC is considered in this article, and the detailed discussion of the two methods is reported in [10].

However, the main disadvantage of MPCC is that it is a model-based control method, which mainly relies on accurate motor parameters to predict current values at the next moment. In reality, the motor parameters may not match their real values because of the influence of motor temperature during operation or the off-line measurement errors [17]–[19]. The mismatch will lead to inaccurate system prediction behaviors, such as increased torque ripples or current tracking errors.

To deal with parameter uncertainties, an MPCC method with gray prediction was proposed in [11]. It has a good current response and anti-interference ability. However, the gray prediction method is computationally intensive and time-consuming. Then a novel extended state observer was proposed in [12] to suppress inductance mismatch, and the incremental model was adopted to improve the robust performance. In [13], an adaptive disturbance observer was proposed to solve the current oscillation and extend the inductance robust limit. However, this method was only for inductance mismatch and the conditions of resistance and flux mismatches were not considered. Since the values of predicted current under the disturbances of inductance and rotor flux linkage cannot be compensated satisfactorily, an incremental model was introduced in [12]. The control algorithm can fundamentally solve the influence of the rotor flux linkage mismatch. In addition, a Lyapunov function with online adaptive laws was introduced in [14] to verify the theoretical robustness and stability of the system. To solve the problems of system stability under parameters mismatch, [15] proposed an improved stator current and disturbance observer. However, due to chattering, it is necessary to adjust and select reasonable sliding parameters in simulation and experiment. In addition, like other methods mentioned above, the original motor parameters need to be obtained, which is a motor parameter dependent method.

To get rid of model dependencies, a model free predictive current control (MFCC) was first investigated in [16]. The MFCC can improve the parameter robustness caused by parameter mismatch without utilizing any initial motor parameters. The problem of mismatch between the inverter and the drive motor is greatly simplified in MFCC and is suitable for different manufacturers. However, this method needs to sample twice in each sampling period, and the instantaneous switching inside the inverter will result in undesirable current spikes. In addition, the previous current variations with the same switching state need be stored in the microprocessor. If a conduction mode has not been updated within several dozens of time intervals, a stagnant current update will occur, that is, limiting current prediction and increasing torque ripple. The same problems also occurred in [17]–[19], which utilized the previous current update errors with a weight factor to improve the control performance. However, the stagnant conduction problem has not been eliminated.

To avoid the detection of undesirable current spikes, a measurement method of sampling the current once in each sampling period was adopted in [20], which greatly simplifies the implementation. In addition, to solve the stagnant current update mechanism, a simple solution was added. The logical judgment was that if a conducting mode was still used within 50 sampling periods, the switching state will be forcibly changed in the next action. However, this switching state maybe undesired. By frequently updating the look-up tables (LUTs), three adjacent feeding voltages are used in [21], [22] to construct all possible current variations. In particular, to reconstruct the LUTs, there are 210 possible vector sequences need to be considered. Some studies of MFCC based on ultra-local model [23] have been applied to PMSM drive systems [24], [25]. However, these methods suffer from complex tuning work and the performance may deteriorate at relatively low sampling frequency. An improvement was proposed in [26], using an ultra-local model structure with an extended state observer to predict the system behavior. However, the initial inductance parameter mismatch can still decrease the control performance of MFCC.

B. MOTIVATION AND INNOVATION

To enhance the current performance, a novel algorithm based on the current update mechanism was proposed in [27]. The algorithm reconstructs the prediction model based on the two most adjacent current variations to improve prediction performance, but the original motor parameters need to be involved, which is a model-based current control method. Different from [27], a new current prediction error model with decoupling of motor parameters is deduced in our paper and there is no initial motor parameters involved in the prediction model compared with [27]. The main contributions are shown as follows:

1) A new current prediction error model is derived based on MPCC method. By analyzing the minimum approximate terms of current error variations, the current prediction error model is deduced, which is helpful to realize the decoupling of stator resistance and inductance. This current prediction error model is an improvement of MPCC method.

2) The decoupling of motor parameters is realized without utilizing any initial motor parameters, and only the measured data is needed. The rotor flux linkage is obtained by bringing the separated stator resistance and inductance into the motor mathematical equation. In this case, the decoupling of three motor parameters is completed respectively. The technique we proposed in this article is inherently a model-free paradigm.

3) A novel MFCC method with the online motor parameter identification is proposed. This proposed MFCC method takes advantage of mathematical relationships in the current prediction error model, and the motor parameters can be updated within each control period to improve the parameter robustness. The simulation and experimental comparisons are carried out with the traditional MPCC and the MFCC method in [20].

C. PAPER ORGANIZATION

The organizational structure of this article is as follows. Section II introduces the traditional MPCC control strategy. Section III presents the basic principles of MFCC, and then proposes an improved MFCC method. Section IV carries out simulation research. Section V compares the experimental results under different parameter disturbances. Section V presents the conclusion.

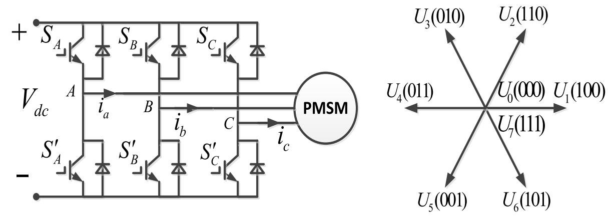

FIGURE 1. The voltage source inverter and candidate voltage vectors.

II. MODEL PREDICTIVE CURRENT CONTROL

A. SPMSM INTRODUCTION

The mathematical and mechanical equations of SPMSM in the rotating coordinate system [28] are expressed as follows:

$$U_d = Ri_d + L\frac{di_d}{dt} - \omega_e L i_q \tag{1}$$

$$U_q = Ri_q + L\frac{di_q}{dt} + \omega_e L i_d + \omega_e \psi_m \tag{2}$$

$$T_e = 1.5p\psi_m i_q \tag{3}$$

$$T_e - T_l = \eta\frac{d\omega_m}{dt} + B\omega_m \tag{4}$$

where U_d, U_q, i_d, and i_q are the stator voltages and stator currents on d-axis and q-axis, respectively; L, Ψ_m, and R are the stator inductance, rotor flux linkage, and stator resistance, respectively; ρ, T_l, ω_m, η, ω_e T_e, and B are the number of pole pairs, load torque, mechanical speed, machine inertia, electrical angular speed, electromagnetic torque, and viscous friction coefficient, respectively. Fig. 1 shows a two-level voltage source inverter for the electric drive system. The eight candidate voltage vectors are described as follow:

$$U_s = \frac{2}{3}V_{dc}(S_A + S_B e^{j\frac{2\pi}{3}} + S_C e^{j\frac{4\pi}{3}}) \tag{5}$$

where $U_s(k)_{sw=i}(i = 0, 1, 2 \ldots, 7)$ are the candidate voltage vectors; V_{dc} is the DC bus voltage; S_A, S_B, and S_C are the switching states of the inverter.

B. MPCC STRATEGY

The principle of MPCC is to predict the expected current behavior in a future time window by minimizing a cost function. According to the first-order Euler discretization method, the predicted d-q axis currents at $(k+1)$ *th* instant can be acquired as

$$\begin{cases} i_d(k+1) = i_d(k) + \dfrac{T_s}{L}U_d(k) - \dfrac{T_s R}{L}i_d(k) \\ \qquad + T_s\omega_e(k)i_q(k) \\ i_q(k+1) = i_q(k) + \dfrac{T_s}{L}U_q(k) - \dfrac{T_s R}{L}i_q(k) \\ \qquad - T_s\omega_e(k)i_d(k) - \dfrac{T_s\psi_m}{L}\omega_e(k) \end{cases} \tag{6}$$

where k is the discrete-time index. Considering the electromagnetic time constant of SPMSM is much smaller than the mechanical time constant, we could regard ω_e as a constant within adjacent sampling periods.

$$\omega_e(k) \approx \omega_e(k+1) \tag{7}$$

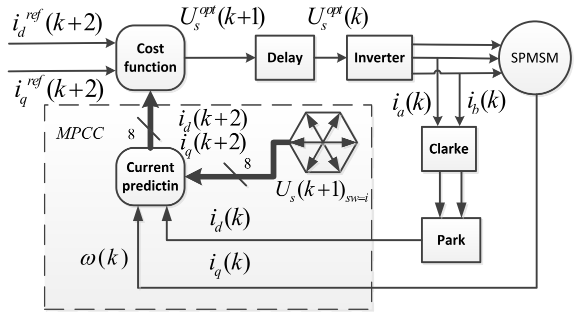

FIGURE 2. The diagram of MPCC method.

In addition, considering the one-step delay compensation strategy in practical electric drive applications [29], the $(k+2)$ *th* instant predicted currents on d-q axis are presented as follows:

$$\begin{cases} i_d(k+2) = i_d(k+1) + \dfrac{T_s}{L}U_d(k+1)_{s=i} \\ \qquad - \dfrac{T_s R}{L}i_d(k+1) + T_s\omega_e(k)i_q(k+1) \\ i_q(k+2) = i_q(k+1) + \dfrac{T_s}{L}U_q(k+1)_{sw=i} \\ \qquad - \dfrac{T_s R}{L}i_q(k+1) - T_s\omega_e(k)i_d(k+1) \\ \qquad - \dfrac{T_s\psi_m}{L}\omega_e(k) \end{cases} \tag{8}$$

Finally, the optimal voltage vector $U_s^{opt}(k)$ in (5) is selected by minimizing the cost function J. The MPCC cost function J is expressed as follows:

$$J = \left|i_d^{ref}(k+2) - i_d(k+2)\right| + \left|i_q^{ref}(k+2) - i_q(k+2)\right| \tag{9}$$

where $i_d^{ref}(k+2)$ and $i_q^{ref}(k+2)$ are the d-axis and q-axis reference currents at $(k+2)$ *th* instant, respectively. Therefore, the optimal voltage vector $U_s^{opt}(k)$ can be obtained by (9). The diagram of traditional MPCC is displayed in Fig. 2.

III. MODEL-FREE PREDICTIVE CURRENT CONTROL

It can be seen from (6) and (8) that the MPCC is a model-based control method, and the accuracy of the predicted currents is affected by motor parameters such as flux linkage, inductance, and resistance. To get rid of model dependencies, a model free control method is proposed, which can suppress multi parameter disturbances without using the model parameters.

In this section, the principle of MFCC [20] is shown in Section A. Then, the shortage of MFCC is explained in Section B. In addition, the proposed error variations model is deduced in Section C. Finally, a novel IMFCC method with the real-time identification is introduced in Section D.

A. PRINCIPLE OF MFCC

To describe MFCC clearly, based on (6), the d-q axis current variations are presented as follows (10), as shown at the bottom of the next page.

The estimated current in MFCC method are expressed as

$$\begin{cases} i_d(k+1) = i_d(k) + \Delta i_{d,old}(k) \\ i_q(k+1) = i_q(k) + \Delta i_{q,old}(k) \end{cases} \tag{11}$$

where $i_d(k+1)$ and $i_q(k+1)$ are the estimated current at $(k+1)$ *th* instant under the voltage vector applied in *kth* instant, respectively; $\Delta i_{d,old}(k)$ and $\Delta i_{q,old}(k)$ refer to the previous current variations with the same switching state stored in the microprocessor. Considering the one-step delay compensation, the predicted $(k+2)$ *th* instant currents are acquired as

$$\begin{cases} i_d(k+2) = i_d(k+1) + \Delta i_{d,old}(k+1)_{sw=i} \\ i_q(k+2) = i_q(k+1) + \Delta i_{q,old}(k+1)_{sw=i} \end{cases} \tag{12}$$

B. LIMITATION OF MFCC

Equations (11) and (12) show that the estimated current expression does not use any motor parameters, and only the stator current and the previous current variations need to be available. However, the application of the MFCC method depends on the following assumptions. The two current variations in (10) and (11) should be very close if the same conduction mode is applied at two different time instants, namely $\Delta i_{dq}(k) \approx \Delta i_{dq,old}(k)$. Since the T_s is much shorter than ω_e, the values of term 1 and 2 could be regarded as constant over several sampling periods. However, if the conduction mode has not been updated within dozens of sampling periods, the values of term 1 and 2 could not be considered the same, resulting in the increasing errors between $\Delta i_{dq}(k)$ and $\Delta i_{dq,old}(k)$. Then, the stagnant current update will occur, and will negatively affect the current prediction accuracies. Therefore, a simple anti-stagnation mechanism has been added in [20]. The logical judgment is that if a conducting mode is still used within 50 successive periods, the switching state will be forcibly changed in the next action. However, since the minimum updating frequency is related to the defined time, the improvement of the stagnation problem is limited. In addition, considering that the switching state maybe undesired, $U_s^{opt}(k)$ might not be optimum according to (12) and (9), which further deteriorates the prediction performance.

C. PRINCIPLE OF IMFCC

To improve the current prediction accuracy, the IMFCC method is proposed in this article. According to (10), the current variations $\Delta i_d(k-1)$ and $\Delta i_q(k-1)$ can be obtained as

$$\begin{cases} \Delta i_d(k-1) = i_d(k-1) - i_d(k-2) \\ = \dfrac{T_s}{L} U_d(k-2) - \dfrac{T_s R}{L} i_d(k-2) + T_s\omega_e(k-2) i_q(k-2) \\ \Delta i_q(k-1) = i_q(k-1) - i_q(k-2) \\ = \dfrac{T_s}{L} U_q(k-2) - \dfrac{T_s R}{L} i_q(k-2) - T_s\omega_e(k-2) i_d(k-2) \\ -\dfrac{T_s\psi_m}{L}\omega_e(k-2) \end{cases} \tag{13}$$

Subtracting (13) from (10), the contiguous instant current variations can be expressed as (14), as shown at the bottom of the next page.

As mentioned in (7), since $\omega_e(k-1) \approx \omega_e(k-2)$, the value of term 5 in (14) can be regarded as zero. Similarly, the term 3 can be approximately expressed as follows:

$$\begin{aligned} &T_s[\omega_e(k-1) i_q(k-1) - \omega_e(k-2) i_q(k-2)] \\ &\quad \approx T_s\omega_e(k-1)[i_q(k-1) - i_q(k-2)] \\ &\quad \approx T_s\omega_e(k)[i_q(k-1) - i_q(k-2)] \\ &\quad = T_s\omega_e(k)\Delta i_q(k-1) \end{aligned} \tag{15}$$

In the similar way, the term 4 can also be obtained approximately as follows:

$$\begin{aligned} &T_s[\omega_e(k-1) i_d(k-1) - \omega_e(k-2) i_d(k-2)] \\ &\quad \approx T_s\omega_e(k-1)[i_d(k-1) - i_d(k-2)] \\ &\quad \approx T_s\omega_e(k)[i_d(k-1) - i_d(k-2)] \\ &\quad = T_s\omega_e(k)\Delta i_d(k-1) \end{aligned} \tag{16}$$

Afterwards, substituting (15) and (16) into (14), the modified equation are expressed as follows:

$$\begin{cases} \Delta i_d(k) - \Delta i_d(k-1) \\ = \dfrac{T_s}{L}[U_d(k-1) - U_d(k-2)] - \dfrac{T_s R}{L}\Delta i_d(k-1) \\ \qquad + T_s\omega_e(k)\Delta i_q(k-1) \\ \Delta i_q(k) - \Delta i_q(k-1) \\ = \dfrac{T_s}{L}[U_q(k-1) - U_q(k-2)] - \dfrac{T_s R}{L}\Delta i_q(k-1) \\ \qquad - T_s\omega_e(k)\Delta i_d(k-1) \end{cases} \tag{17}$$

Finally, by rearranging the (17), the decoupling of stator resistance and inductance are realized as follows (18), as shown at the bottom of the next page.

$$\begin{cases} \Delta i_d(k) = i_d(k) - i_d(k-1) \\ = \dfrac{T_s}{L}[U_d(k-1) - R i_d(k-1)] + \overbrace{T_s\omega_e(k-1) i_q(k-1)}^{\text{Term1}} \\ \Delta i_q(k) = i_q(k) - i_q(k-1) \\ = \dfrac{T_s}{L}[U_q(k-1) - R i_q(k-1)] - \overbrace{[T\omega_e(k-1) i_d(k-1) + \dfrac{T_s}{L}\psi_m\omega_e(k-1)]}^{\text{Term2}} \end{cases} \tag{10}$$

From (18), we observed that the stator resistance and inductance can be decoupled only through the measured data, such as continuous instant current prediction error variations, and the initial rotor flux linkage is no longer involved. Next, the real-time identification of these two parameters will be carried on based on this newly derived current prediction error model, which is also an important step in IMFCC method.

D. PARAMETER IDENTIFICATION BY RLS

In order to obtain accurate motor parameters, the stator resistance and inductance have to be estimated online. The recursive least squares (RLS) algorithm is one of the most widespread methods because of its robustness and simplicity. Here, we adopt the parameter identification method of RLS, and its mathematical expressions are as follows:

$$\begin{cases} y(k) = \varphi^T(k) \cdot \theta(k) \\ \theta(k) = \theta(k-1) + g(k)[y(k) - \varphi^T(k) \cdot \theta(k-1)] \\ g(k) = \dfrac{p(k-1)\varphi(k)}{\lambda I + \varphi^T(k)p(k-1)\varphi(k)} \\ p(k) = \dfrac{1}{\lambda} p(k-1)[I - g(k)\varphi^T(k)] \end{cases} \tag{19}$$

where $y(k)$ is the output matrix; $\varphi(k)$ is the feedback matrix; $\theta(k)$ is the estimated parameter vector; λ is the forgetting factor with a value of 0.99; $g(k)$ and $p(k)$ are correction gain matrices. At the startup, the RLS algorithm is initialized as

$$\begin{cases} \theta(0) = \varepsilon \\ p(0) = \alpha I \end{cases} \tag{20}$$

where ε is a zero vector; the value of α is; I is a second-order identity matrix. According to on (18) and (19), the estimation method of stator inductance and resistance based on RLS can be obtained as follows (21)–(23), as shown at the bottom of the next page, where $\hat{L}(k)$ and $\hat{R}(k)$ are the estimates of stator inductance and resistance at kth instant, respectively. Substituting (21)-(23) into (19), the stator resistance and inductance parameters of the motor can be identified in real-time based on simple recursive least square (RLS). Afterward, substituting the newly identified resistance and inductance into (2), the estimated rotor flux linkage at kth instant can be easily obtained through the newly identified parameters of stator resistance and inductance.

$$\hat{\psi}_m(k) = \frac{U_q(k) - \hat{R}(k)i_q(k) - \hat{L}(k)\frac{di_q(k)}{dt} - \omega_e(k)\hat{L}(k)i_d(k)}{\omega_e(k)} \tag{24}$$

It should be noted that the resistor voltage drop is much smaller than the voltage drop, namely $|Ri_d(k-1)| \ll |U_d(k-1)|$ and $|Ri_q(k-1)| \ll |U_q(k-1)|$. However, if two succeeding similar voltage vectors are applied in the controller, it may lead to inaccurate estimates in (17). Therefore, two situations need to be considered. If the applied voltage vectors $U_{d,q}$(k-1) and $U_{d,q}$(k-2) are not equal, the continuous instant current prediction error variations are updated using (17), and the new current error variations at the current instant will be stored in the microprocessor. Otherwise, the latest instant current prediction error variations in the memory will be utilized until the new current error variations are acquired through (17). Fortunately, a sequence of more than two similar voltage vectors does not occur frequently in an MPCC or MFCC.

Based on the proposed current error variation model, the parameters of flux linkage, inductance, and resistance can be obtained without utilizing any initial motor parameters, and only the stator current and the previous current error

$$\begin{cases} \Delta i_d(k) - \Delta i_d(k-1) \\ = \dfrac{T_s}{L}[U_d(k-1) - U_d(k-2)] - \dfrac{T_sR}{L}[i_d(k-1) - i_d(k-2)] \\ + \overbrace{T_s[\omega_e(k-1)i_q(k-1) - \omega_e(k-2)i_q(k-2)]}^{\text{Term3}} \\ \\ \Delta i_q(k) - \Delta i_q(k-1) \\ = \dfrac{T_s}{L}[U_q(k-1) - U_q(k-2)] - \dfrac{T_sR}{L}[i_q(k-1) - i_q(k-2)] \\ - \overbrace{T_s[\omega_e(k-1)i_d(k-1) - \omega_e(k-2)i_d(k-2)]}^{\text{Term4}} \\ - \overbrace{\dfrac{T_s\psi_m}{L}[\omega_e(k-1) - \omega_e(k-2)]}^{\text{Term5}} \end{cases} \tag{14}$$

$$\begin{bmatrix} U_d(k-1) - U_d(k-2) \\ U_q(k-1) - U_q(k-2) \end{bmatrix} = \begin{bmatrix} \dfrac{1}{T_s}[\Delta i_d(k) - \Delta i_d(k-1)] - \omega_e(k)\Delta i_q(k-1) & \Delta i_d(k-1) \\ \dfrac{1}{T_s}[\Delta i_q(k) - \Delta i_q(k-1)] + \omega_e(k)\Delta i_d(k-1) & \Delta i_q(k-1) \end{bmatrix} \begin{bmatrix} L \\ R \end{bmatrix} \tag{18}$$

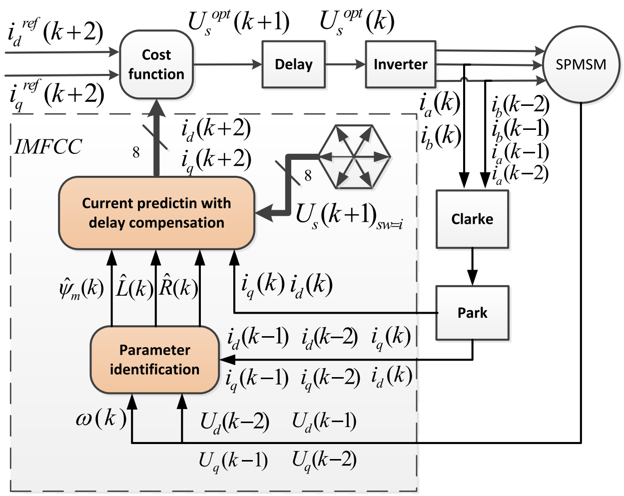

FIGURE 3. The IMFCC method in SPMSM drives.

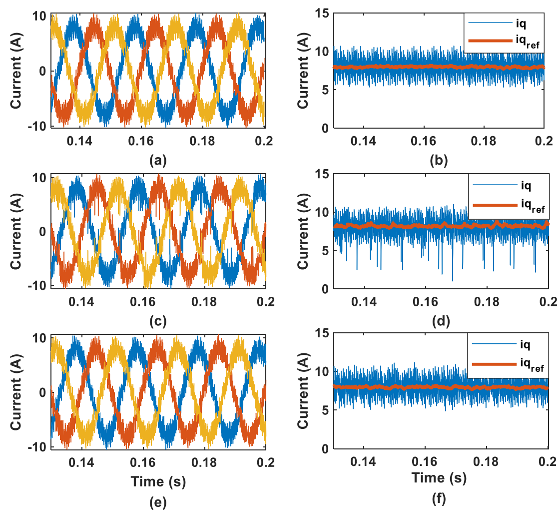

FIGURE 4. Simulation results of current without parametric mismatch. (a) and (b) method 1; (c) and (d) method 2; (e) and (f) method 3.

TABLE 1. PMSM parameters.

Parameter	Description	Value
Ψ_m	Rotor flux linkage	0.1667 (Wb)
L	Stator inductance	1.225 (mH)
R	Stator resistance	0.365 (Ω)
ρ	Number of pole pairs	4
P_N	Rated power	2 (kW)
T_N	Rated torque	10 (Nm)

variations need to be available. The proposed method is a model free paradigm. It can be found that the identified parameters can be updated within each period, which could effectively improve prediction accuracy. After obtaining the identified motor parameters, the predicted currents are acquired as follows:

$$\begin{cases} i_d(k+1) = i_d(k) + \dfrac{T_s}{\hat{L}(k)}U_d(k) - \dfrac{T_s\hat{R}(k)}{\hat{L}(k)}i_d(k) \\ \qquad + T_s\omega_e(k)i_q(k) \\ i_q(k+1) = i_q(k) + \dfrac{T_s}{\hat{L}(k)}U_q(k) - \dfrac{T_s\hat{R}(k)}{\hat{L}(k)}i_q(k) \\ \qquad - T_s\omega_e(k)i_d(k) - \dfrac{T_s\hat{\psi}_m(k)}{\hat{L}(k)}\omega_e(k) \end{cases} \tag{25}$$

Then, the predicted currents at $(k+2)$ *th* instant can be acquired in (26). The optimal voltage vector $U_s^{opt}(k)$ is selected by minimizing the cost function J. According to (21)-(26), the system control block diagram of the IMFCC method is displayed in Fig. 3.

$$\begin{cases} i_d(k+2) = i_d(k+1) + \dfrac{T_s}{\hat{L}(k+1)}U_d(k+1)_{sw=i} \\ \qquad - \dfrac{T_s\hat{R}(k+1)}{\hat{L}}i_d(k+1) \\ \qquad + T_s\omega_e(k)i_q(k+1) \\ i_q(k+2) = i_q(k+1) + \dfrac{T_s}{\hat{L}(k+1)}U_q(k+1)_{sw=i} \\ \qquad - \dfrac{T_s\hat{R}(k+1)}{\hat{L}(k+1)}i_q(k+1) \\ \qquad - T_s\omega_e(k)i_d(k+1) - \dfrac{T_s\hat{\psi}_m(k+1)}{\hat{L}(k+1)}\omega_e(k) \end{cases} \tag{26}$$

IV. SIMULATION STUDY

To verify the robustness and driving performance under different parameter disturbances, the three methods are compared in the simulation and experimental environment.

For the convenience of description, the traditional MPCC method is named after Method 1. The modified MFCC method with anti-stagnant current update detection [20] is named after Method 2. The proposed improved MFCC

$$y(k) = \begin{bmatrix} U_d(k-1) - U_d(k-2) \\ U_q(k-1) - U_q(k-2) \end{bmatrix} \tag{21}$$

$$\varphi^T(k) = \begin{bmatrix} \dfrac{1}{T_s}[\Delta i_d(k) - \Delta i_d(k-1)] - \omega_e(k)\Delta i_q(k-1) & \Delta i_d(k-1) \\ \dfrac{1}{T_s}[\Delta i_q(k) - \Delta i_q(k-1)] + \omega_e(k)\Delta i_d(k-1) & \Delta i_q(k-1) \end{bmatrix} \tag{22}$$

$$\theta(k) = \begin{bmatrix} \hat{L}(k) \\ \hat{R}(k) \end{bmatrix} \tag{23}$$

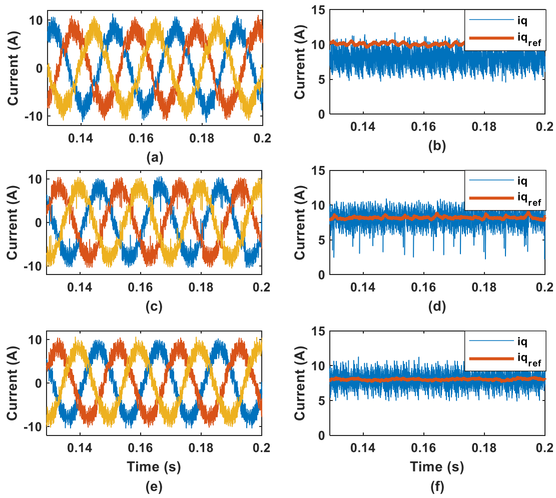

FIGURE 5. Simulation results of current under $L' = 0.5L$, $\Psi'_m = 0.5\Psi_m$, and $R' = 5R$. (a) and (b) method 1; (c) and (d) method 2; (e) and (f) method 3.

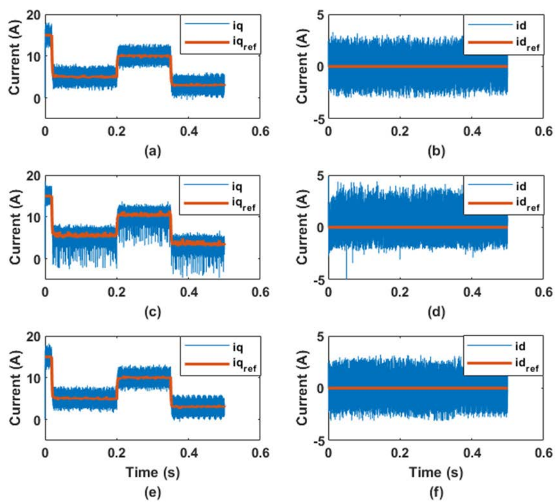

FIGURE 6. Simulation results of current without parametric mismatch at 1000 r/min. (a) method 1; (c) method 2; (d)-(f) and (b) method 3.

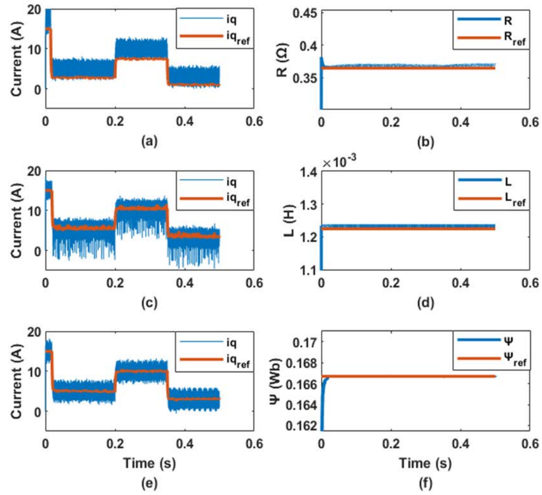

FIGURE 7. Simulation results of current under $L' = 1.5L$, $\Psi'_m = 2\Psi_m$, and $R' = 10R$ at 1000 r/min. (a) method 1; (c) method 2; (d)-(f) and (b) method 3.

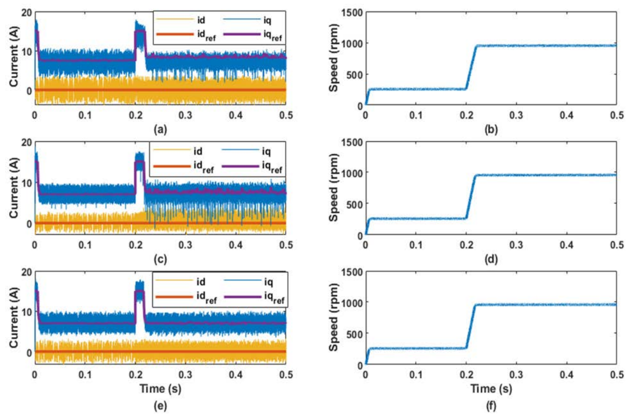

FIGURE 8. Simulation results of measured electromagnetic torque under $L' = 2L$, $R' = 0.1R$, and $\Psi'_m = 1/3\Psi_m$ at different speeds. (a) and (b) method 1; (c) and (d) method 2; (e)-(f) method 3.

method is named after Method 3. The system sampling period is 50μ. Since the driving motor is a surface-mounted PMSM, the $i_d = 0$ current control strategy is adopted. According to the motor parameter values shown in Table 1, the reference torque value is almost equal to the reference current value as follows:

$$T_e^{ref} = 1.5p\psi_m i_q = 1.0002 i_q^{ref} \approx i_q^{ref} \tag{27}$$

The steady performance of three-phase current and torque current i_q without parameter mismatch is observed in Fig. 4. The reference current is set to 8 A at 800 r/min. It can be seen from Fig. 4 (b), (d) and (f) that the torque current i_q can stably track the reference values in the three methods. However, method 2 has some current ripples due to the stagnant current update mechanism. The total harmonic distortions (THDs) of the stator currents in Fig. 4 (a), (b) and (c) are 34.06%, 36.07%, 34.42%, respectively. Fig. 5 shows the steady performance under multi parameter mismatch. It can be seen that in Fig. 5(b), there are some offsets between the measured current i_q and the reference current, because method 1 is a motor parameter dependent control method, and the multi parameter mismatch of the motor may cause current prediction errors, as shown in (8). The THDs of the three methods are 45.77%, 36.17%, 34.59%, respectively. It can be seen that method 3 has the best current performance in both suppressing torque ripple and tracking the given values, and also has the lowest current harmonic.

The dynamic torque current results without parameter mismatch are observed in Fig. 6. The given torque current i_q rises from 5 to 10 A at 0.2 s, and then drops to 3 A at 0.35 s at 1000r/min. From the results, there is a certain current fluctuation in the predicted current of method 2 due to the stagnant current update mechanism. Fig. 7 shows the dynamic performance of the three methods under multi parameter mismatches. The given torque current i_q also rises from 5 to 10 A

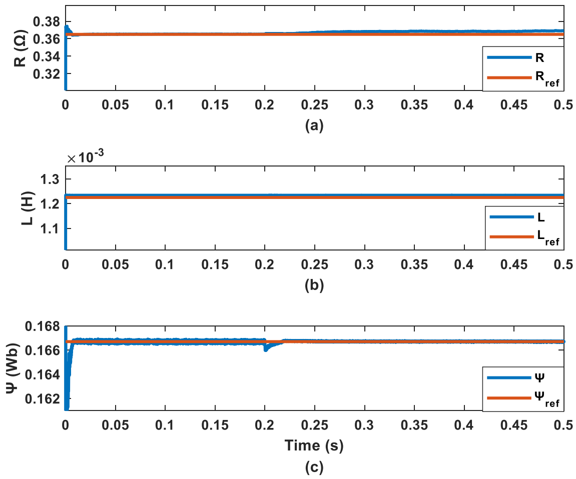

FIGURE 9. Simulation results of identified rotor flux linkage, stator resistance, and stator inductance under $L' = 2L$, $R' = 0.1R$, and $\Psi'_m = 1/3\Psi_m$ at different speed.

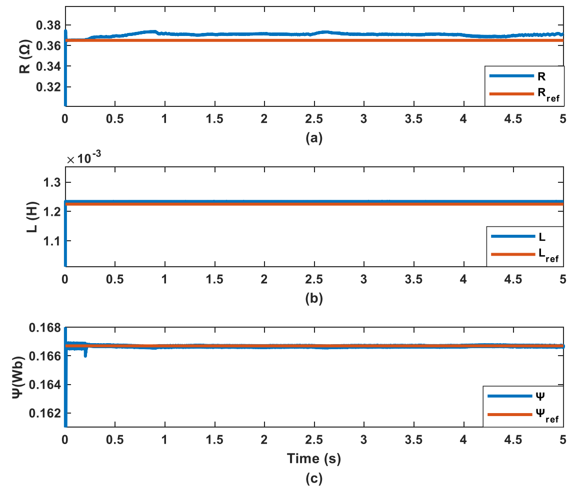

FIGURE 10. Simulation results of identified rotor flux linkage, stator resistance, and stator inductance under $L' = 2L$, $R' = 0.1R$, and $\Psi'_m = 1/3\Psi_m$ at different speed.

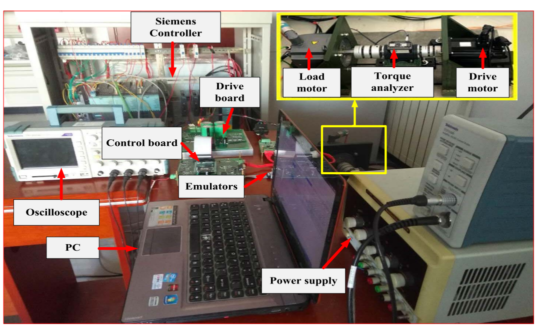

FIGURE 11. Experimental platform for SPMSM drives.

at 0.2 s, and then drops to 3 A at 0.35 s at 1000r/min. Method 1 shows that there is certain offset between the measured current and the given value. This is because the prediction errors caused by parameter uncertainties could not be compensated satisfactorily, which ultimately leads to inaccurate current

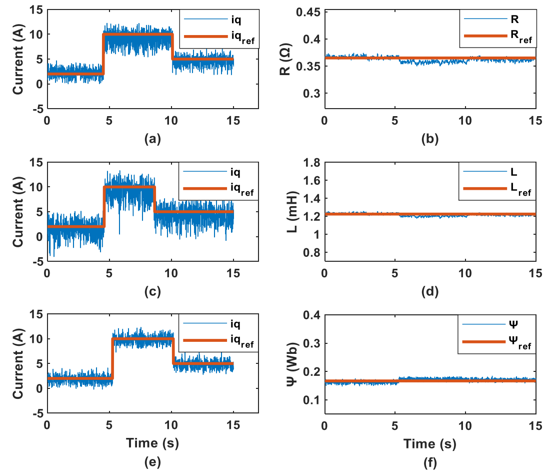

FIGURE 12. Experimental results under $L' = 0.5L$. (a) method 1; (c) method 2; (d)-(f) and (b) method 3.

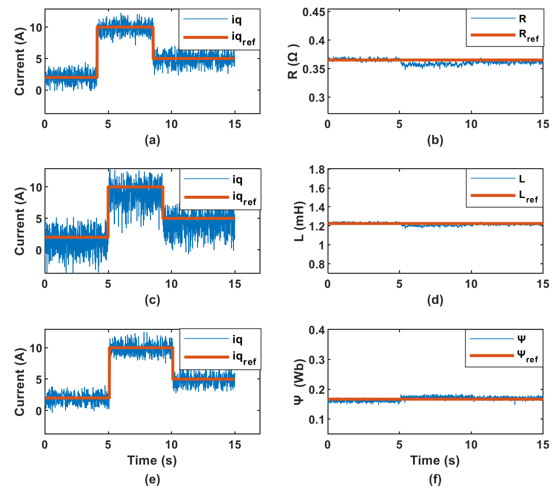

FIGURE 13. Experimental results under $L' = 2L$ at 800 r/min. (a) method 1; (c) method 2; (d)-(f) and (b) method 3.

predictions. We can observe that the parameters of flux linkage, inductance, and resistance in Fig. 7 basically maintain the robust identification results regardless of the torque step signals, and are also very close to the real values. Compared with the other two methods, the Method 3 has the best current performance in terms of torque ripple suppression or tracking the given values. This is because this novel method takes advantage of mathematical relationships in the current prediction error model, and the identified motor parameters can be updated within each period to improve prediction accuracy.

In addition, Fig. 8 shows the dynamic torque current results under multi parameter disturbances and different speeds conditions. The motor starts with a constant load torque of 7 Nm, and then increases the motor speed from 300 to 1000 r/min at 0.2 s. We can observe that the torque ripple in Method1 and Method 2 are relatively larger than that in method 3. The identified values of the three motor parameters can well track the real values in Fig. 9. By the way, it can be concluded from (24) that the motor speed has a certain influence on the

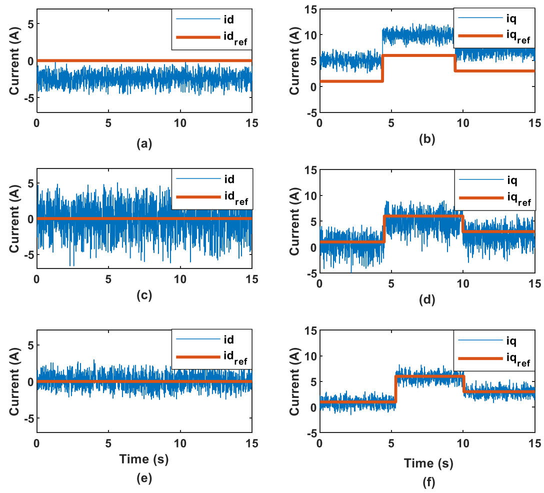

FIGURE 14. Experimental results at 800 r/min under $\Psi_m' = 2\Psi_m$. (a) and (b) method 1; (c) and (d) method 2; (e) and (f) method 3.

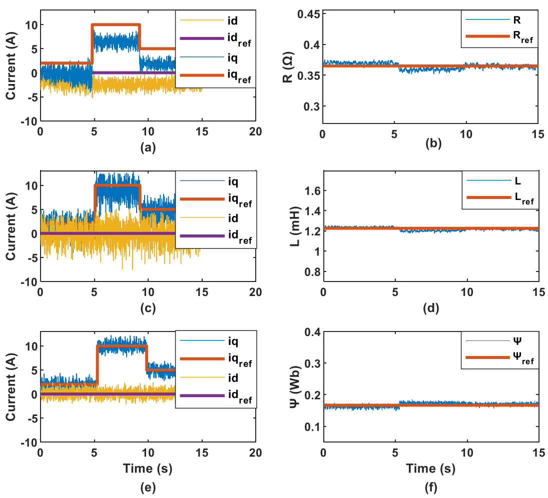

FIGURE 15. Experimental results at 800r/min under $\Psi_m' = 1/3\Psi_m$. (a) and (b) method 1; (c) and (d) method 2; (e) and (f) method 3.

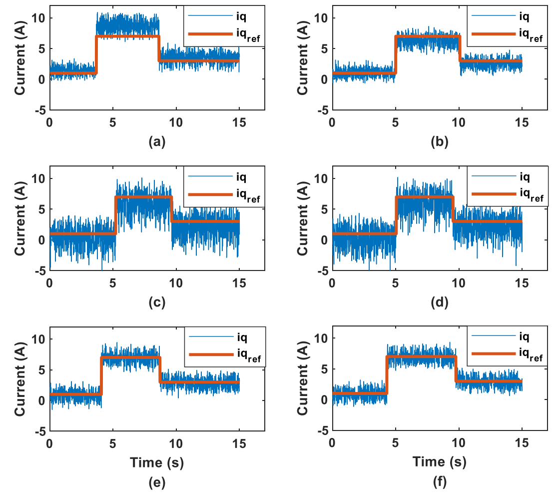

FIGURE 16. Experimental results at 800 r/min. (a) method 1 with $R' = 10R$; (b) method 1 with $R' = 0.1R$; (c) method 2 with $R' = 10R$; (d) method 2 with $R' = 0.1R$; (e) method 3 with $R' = 10R$; (f) method 3 with $R' = 0.1R$.

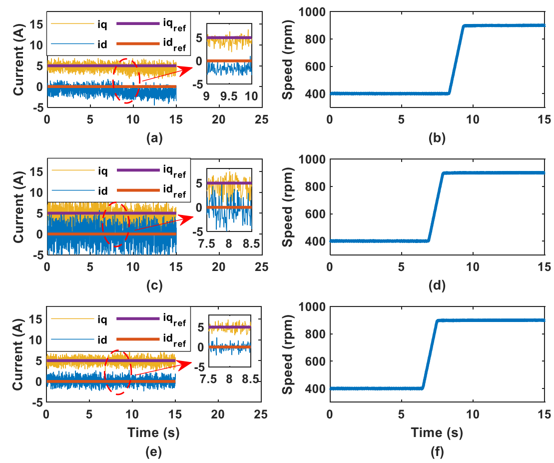

FIGURE 17. Experimental results of the current and speed response under $L' = 2L$, $R' = 10R$, and $\Psi_m' = 0.5\Psi_m$ at different speeds. (a) and (b) method 1; (c) and (d) method 2; (e) and (f) method 3.

accuracy of flux linkage identification. As shown in Fig. 9(c), the identified flux linkage has a small fluctuation under the speed step signal at 0.2s. This is because the electromagnetic time constant of the SPMSM is much smaller than ω_e, resulting in identification lag phenomenon. In addition, we can find that compared with low speed, the flux identification effect is better at higher speed of 1000 r/min. In order to further show the identification effect, the identification results of the motor parameters for 0-5s are given in Fig.10. The identification errors of motor resistance, inductance and flux linkage at 0.5-5s are 2.25%, 0.73% and 0.06%, respectively. We can observe that the IMFCC method maintains a relatively robust identification effect in the simulation, and the identification results are also very close to the real values.

V. EXPERIMENTAL RESULTS

As shown in Fig. 11, an experimental platform is established. The test platform includes a load motor, drive motor, control board, drive board, power supply (310V/10A), oscilloscope, auxiliary power supply (15V/2A), and the emulator. The power of the load motor is 5.6 kW, and the drive motor is 2 kW. The main control chip is a TMS320F28337d, and the power module is FNC42060F-type. The system sampling frequency is 20 kHz, and the dead time is set to 2.5μs. Table 1 shows the main parameter values of SPMSM.

In the following experiment, the robustness performance of three methods under parameter mismatch conditions is observed. Fig. 12 shows the experimental results at 800 r/min under $L' = 0.5L$ condition. The reference torque current i_q rises from 2 to 10 A, and then drops to 5A. Fig. 12(a) shows some offsets between the given current and the measured torque current, which also proves that the inductance mismatch affects the tracking effect. Due to the stagnant current update detection in MFCC, the predicted current of method 2 has certain current fluctuations and spikes. Table 2

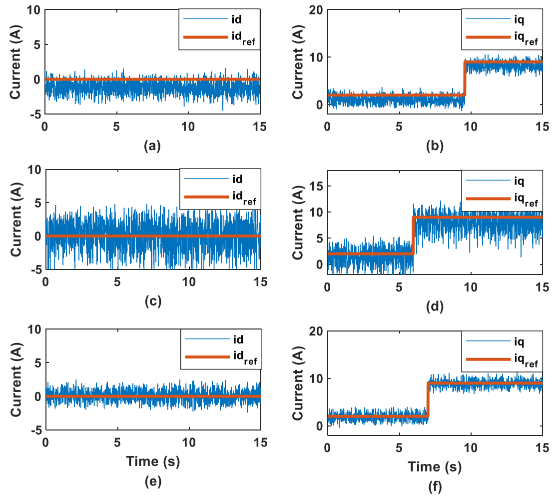

FIGURE 18. Experimental results under $L' = 2L$, $R' = 5R$, and $\Psi'_m = 0.5\Psi_m$. (a) and (b) method 1; (c) and (d) method 2; (e) and (f) method 3.

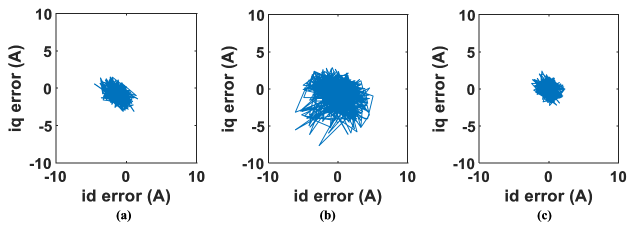

FIGURE 19. Experiment results of currents error at 800 r/min under $R' = 20R$, $L' = 1.5L$ and $\Psi'_m = 1.5\Psi_m$. (a) method 1; (b) method 2; (c) method 3.

shows the torque ripple value of the three methods under the given value of 5N at the speed of 800r/min. In Fig. 12, the resistance identification errors under different torque steps are 2.47%, 4.1% and 2.46%, respectively; the inductance identification errors are 2.45%, 3.84% and 2.29%, respectively; the flux identification errors are 9.42%, 8.58% and 6.18%, respectively.

Similarly, Fig. 13 shows the experimental results under $L' = 2L$ condition at 800 r/min. The torque current rises from 2 to 10A, and then down to 5A. The resistance identification errors under different torque steps are 1.64%, 3.94% and 1.92%, respectively; the inductance identification errors are 1.88%, 3.92% and 2.37%, respectively; the flux identification errors are 7.62%, 7.38% and 5.22%, respectively. Fig. 12 and 13 show that the identified motor parameters fluctuate slightly with the torque step, but basically close to the actual value, and the identified errors are acceptable.

Fig. 14 shows the current robustness performance under $\Psi_m = 2\Psi_m$ condition at 800 r/min. The torque current rises from 1 to 6A, and then down to 3A. We can observe that in Fig. 14(a) and (b), the measured currents i_d and i_q are obviously higher than the given current. This is because method 1 is a model-based control algorithm, which leads to the cost function errors under flux linkage mismatch conditions, and eventually causes in offset with the reference. In method 2,

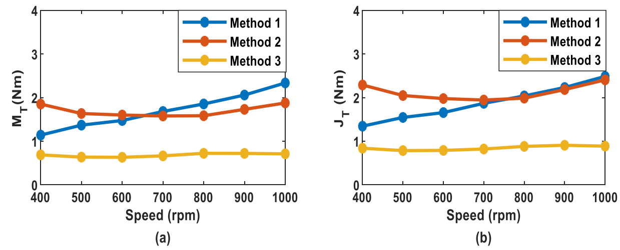

FIGURE 20. Experimental results of M_T and J_T under $L' = 2L$, $\Psi'_m = 1.5\Psi_m$, and $R' = 10R$ at different speeds.

the measured values i_d and i_q can track the reference values better than method 1, because method 2 is a model-free control algorithm, and the accuracy of the predicted current does not depend on the initial motor parameters. However, due to this stagnant current update, method 2 has some current spikes. Fig. 15 shows similar performance. The reference torque current rises from 2 to 10A, and down to 5A. Similarly, the comparison under $\Psi_m = 1/3\Psi_m$ mismatch condition at 800r/min shows that method 3 has the best robustness performance in terms of tracking the reference and fluctuation range. In the case of flux linkage mismatch and torque step, the three identified parameters can track the real values of parameters faster and more stably, which effectively improves the predictive control performance of method 3.

The driving performance of three methods under $R' = 10R$ and $R' = 0.1R$ conditions, respectively, is shown in Fig. 16. The reference current rises from 1 to 7 A, and down to 3 A. The measured current value obviously exceeds the reference torque current value of 7 A in Fig. 16(a), reaching 9A, which is due to the fact that the predicted current under resistance mismatch cannot be compensated satisfactorily. In Fig. 16 (b), we can observe that the reference current can be well tracked. That is because the reduced resistance value is relatively smaller compared with the speed and voltage terms in (8).

Fig. 17 shows the current control performance at different speeds with multi parameter disturbances. The load torque is set to 5Nm, and the speed considered is increased from 400 to 900 r/min. At low speed, the measured currents i_d and i_q can track the given values in method 1, but when the speed rises to 900 r/min, the measured currents are significantly lower than the given values. According to (6), the reason for the inaccurate current prediction is the increase of the back EMF of the motor, and considering the prediction error caused by the multi parameter mismatch, the predicted current cannot be further compensated satisfactorily. Method 2 can track the given values well at different speeds, but it has some current ripples, which is due to the stagnant current update mechanism. Table 2 shows the torque ripple values of the three methods under the given value of 5N at the speed of 900r/min. It can be seen that the method 3 has the best current performance in terms of torque ripple suppression or tracking the given values.

TABLE 2. Torque ripple comparisons of different methods.

Different conditions	Evaluation method	Method 1	Method 2	Method 3
$T^*=5$ N, L'=0.5L at 800 r/min	M_T	0.8082	1.5323	0.7273
	J_T	1.0417	1.8930	0.8877
$T^*=7$ N, R'=10R at 800 r/min	M_T	1.7346	1.7056	0.7834
	J_T	1.9616	2.0982	0.9636
$T^*=6$ N, Ψ'_m=2Ψ_m at 800 r/min	M_T	4.0347	1.6611	0.7177
	J_T	4.1378	2.0860	0.8902
$T^*=5$ N, L'=2L, R'=10R, and Ψ'_m=0.5Ψ_m at 900 r/min	M_T	1.0008	1.8221	0.7359
	J_T	1.2411	2.3011	0.9137
$T^*=4$ N, L'=2L, R'=20R, and Ψ'_m=1.5Ψ_m at 800 r/min	M_T	2.6938	1.5571	0.7515
	J_T	2.8212	1.9830	0.8951

TABLE 3. Computation time of three methods.

Method	Method 1	Method 2	Method 3
Computation time	20.23μs	21.35μs	24.68μs

Fig. 18 presents the experimental results of three methods under $R' = 5R$, $L' = 2L$, and $\Psi_m = 0.5\Psi_m$ mismatch conditions. The reference torque current i_q rises from 2 to 9 A at 800 r/min. Due to the stagnation current update detection, Method 2 has some current spikes, but its measured values i_d and i_q can track the reference values better than method 1. Method 3 takes advantage of mathematical relationships in the current prediction error model, and the identified motor parameters can be updated within each period to improve prediction accuracy, which is a novel anti-stagnant current update detection mechanism in MFCC.

The current errors between the given and measured current of three methods under multi-parameter mismatch conditions are shown in Fig.19. Compared with method 1, method 3 can track the reference better because the Fig. 19(c) is close to a circle, and we can also observe that method 3 has relatively small current errors. In addition, to quantitatively examine the torque ripple performance, the two-assessment criterion are presented as follows [17], [20]:

$$M_T = \frac{1}{N}\sum_{k=1}^{N}|e(k)| = \frac{1}{N}\sum_{k=1}^{N}\left|T^*_{(k)} - T_{(k)}\right| \tag{28}$$

$$J_T = \sqrt{\frac{1}{N}\sum_{k=1}^{N}(T^*_{(k)} - T_{(k)})^2} \tag{29}$$

where $T^*_{(k)}$, $T_{(k)}$, and N represent reference torque, measured electromagnetic torque, and the total number of sampling calculation points, respectively. Fig. 20 shows that M_T and J_T of the three methods with multi parameter mismatch at different speeds conditions. We can observe that the method 3 has the lowest torque ripple.

To enhance the contrast, the torque ripple comparisons of three methods under different parameter mismatch are presented in Table 2. These results clearly demonstrate the effectiveness of the proposed method. The computation time of three methods using the Code Composer Studio 8.2.0 software is listed in Table 3. Due to the real-time update identification of RLS method, the computation time of the IMFCC method is slightly longer than that of other methods, but it has the best parameter robustness under different parameter disturbances.

VI. CONCLUSION

To get rid of the stagnant current update mechanism, a novel MFCC method with the real-time identification of motor parameters is proposed. In order to verify the control performance of the electric drive system under parameter mismatch conditions, different load torques, and different rotation speed are implemented. Simulation and experimental results show that this proposed method has the best current performance compared with other two methods either in tracking the reference or in current fluctuation range. Similarly, the results show that the identified motor parameters can track the real values well, which also directly verify the correctness of the proposed method. In addition, to verify the torque ripple performance, the torque ripple assessment criterion are presented in the experiment. The results also show that the proposed method can effectively reduce torque ripple under parameter uncertainties. Therefore, this method can effectively improve the performance of MFCC, and could be applied in SPMSM drivers.

In terms of the future MFCC difficulties and challenges, the current quantization noise is a main possible barrier. To deal with this issue, advanced current sampling technologies should be developed and designed.

REFERENCES

[1] S. Kouro, P. Cortes, R. Vargas, U. Ammann, and J. Rodriguez, "Model predictive control—A simple and powerful method to control power converters," *IEEE Trans. Ind. Electron.*, vol. 56, no. 6, pp. 1826–1838, Jun. 2009.

[2] K. Yin, L. Gao, R. Chen, Z. Feng, and S. Liu, "Adaptive deadbeat predictive current control for PMSM with feed forward method," *IEEE Access*, vol. 9, pp. 101300–101310, 2021.

[3] J. Rodríguez, M. P. Kazmierkowski, J. R. Espinoza, P. Zanchetta, H. Abu-Rub, H. A. Young, and C. A. Rojas, "State of the art of finite control set model predictive control in power electronics," *IEEE Trans. Ind. Informat.*, vol. 9, no. 2, pp. 1003–1016, May 2013.

[4] F. Niu, X. Wang, S. Huang, X. Huang, L. Wu, K. Li, and Y. Fang, "Current prediction error reduction method of predictive current control for permanent magnet synchronous motors," *IEEE Access*, vol. 8, pp. 124288–124296, 2020.

[5] T. Geyer, G. Papafotiou, and M. Morari, "Model predictive direct torque control—Part I: Concept, algorithm, and analysis," *IEEE Trans. Ind. Electron.*, vol. 56, no. 6, pp. 1894–1905, Jun. 2009.

[6] Y. Zhang, Z. Yin, W. Li, J. Liu, and Y. Zhang, "Adaptive sliding-mode-based speed control in finite control set model predictive torque control for induction motors," *IEEE Trans. Power Electron.*, vol. 36, no. 7, pp. 8076–8087, Jul. 2021.

[7] J. Gao, C. Gong, W. Li, and J. Liu, "Novel compensation strategy for calculation delay of finite control set model predictive current control in PMSM," *IEEE Trans. Ind. Electron.*, vol. 67, no. 7, pp. 5816–5819, Jul. 2020.

[8] J. Falck, G. Buticchi, and M. Liserre, "Thermal stress based model predictive control of electric drives," *IEEE Trans. Ind. Appl.*, vol. 54, no. 2, pp. 1513–1522, Mar. 2018.

[9] H. A. Young, A. Perez, and J. Rodriguez, "Analysis of finite-control-set model predictive current control with model parameter mismatch in a three-phase inverter," *IEEE Trans. Ind. Electron.*, vol. 63, no. 5, pp. 3100–3107, May 2016.
[10] S. Vazquez, J. Rodriguez, M. Rivera, L. G. Franquelo, and M. Norambuena, "Model predictive control for power converters and drives: Advances and trends," *IEEE Trans. Ind. Electron.*, vol. 64, no. 2, pp. 935–947, Feb. 2017.
[11] W. Tu, G. Luo, R. Zhang, Z. Chen, and R. Kennel, "Finite-control-set model predictive current control for PMSM using grey prediction," in *Proc. IEEE Energy Convers. Congr. Expo.*, Sep. 2016, pp. 1–7.
[12] M. Yang, X. Lang, J. Long, and D. Xu, "Flux immunity robust predictive current control with incremental model and extended state observer for PMSM drive," *IEEE Trans. Power Electron.*, vol. 32, no. 12, pp. 9267–9279, Dec. 2017.
[13] R. Yang, M.-Y. Wang, L.-Y. Li, C.-M. Zhang, and J.-L. Jiang, "Robust predictive current control with variable-gain adaptive disturbance observer for PMLSM," *IEEE Access*, vol. 6, pp. 13158–13169, 2018.
[14] H. T. Nguyen and J.-W. Jung, "Finite control set model predictive control to guarantee stability and robustness for surface-mounted PM synchronous motors," *IEEE Trans. Ind. Electron.*, vol. 65, no. 11, pp. 8510–8519, Nov. 2018.
[15] X. Zhang, B. Hou, and Y. Mei, "Deadbeat predictive current control of permanent-magnet synchronous motors with stator current and disturbance observer," *IEEE Trans. Power Electron.*, vol. 32, no. 5, pp. 3818–3834, May 2017.
[16] C.-K. Lin, T.-H. Liu, J.-T. Yu, L.-C. Fu, and C.-F. Hsiao, "Model-free predictive current control for interior permanent-magnet synchronous motor drives based on current difference detection technique," *IEEE Trans. Ind. Electron.*, vol. 61, no. 2, pp. 667–681, Feb. 2014.
[17] C. Lin, J. Yu, H. Yu, and Y. Lo, "Simplified model-free predictive current control for synchronous reluctance motor drive systems," in *Proc. IEEE Int. Magn. Conf.*, May 2015, p. 1.
[18] M. Siami, D. A. Khaburi, A. Abbaszadeh, and J. Rodríguez, "Robustness improvement of predictive current control using prediction error correction for permanent-magnet synchronous machines," *IEEE Trans. Ind. Electron.*, vol. 63, no. 6, pp. 3458–3466, Jun. 2016.
[19] M. Siami, D. A. Khaburi, and J. Rodíguez, "Torque ripple reduction of predictive torque control for PMSM drives with parameter mismatch," *IEEE Trans. Power Electron.*, vol. 32, no. 9, pp. 7160–7168, Sep. 2017.
[20] C.-K. Lin, J.-T. Yu, Y.-S. Lai, and H.-C. Yu, "Improved model-free predictive current control for synchronous reluctance motor drives," *IEEE Trans. Ind. Electron.*, vol. 63, no. 6, pp. 3942–3953, Jun. 2016.
[21] D. Da Ru, M. Polato, and S. Bolognani, "Model-free predictive current control for a SynRM drive based on an effective update of measured current responses," in *Proc. IEEE Int. Symp. Predictive Control Electr. Drives Power Electron. (PRECEDE)*, Sep. 2017, pp. 119–124.
[22] P. G. Carlet, F. Tinazzi, S. Bolognani, and M. Zigliotto, "An effective model-free predictive current control for synchronous reluctance motor drives," *IEEE Trans. Ind. Appl.*, vol. 55, no. 4, pp. 3781–3790, Jul./Aug. 2019.
[23] M. Fliess and C. Join, "Model-free control and intelligent PID controllers: Towards a possible trivialization of nonlinear control?" *IFAC Proc. Volumes*, vol. 42, no. 10, pp. 1531–1550, 2009.
[24] Y. Zhou, H. Li, and H. Yao, "Model-free control of surface mounted PMSM drive system," in *Proc. IEEE Int. Conf. Ind. Technol. (ICIT)*, Mar. 2016, pp. 175–180.
[25] Y. Zhou, H. Li, and H. Zhang, "Model-free deadbeat predictive current control of a surface-mounted permanent magnet synchronous motor drive system," *J. Power Electron.*, vol. 18, no. 1, pp. 103–115, Jan. 2018.
[26] Y. Zhang, J. Jin, and L. Huang, "Model-free predictive current control of PMSM drives based on extended state observer using ultralocal model," *IEEE Trans. Ind. Electron.*, vol. 68, no. 2, pp. 993–1003, Feb. 2021.
[27] X. Yuan, S. Zhang, and C. Zhang, "Improved model predictive current control for SPMSM drives with parameter mismatch," *IEEE Trans. Ind. Electron.*, vol. 67, no. 2, pp. 852–862, Feb. 2020.
[28] Y. Tang, W. Xu, Y. Liu, and D. Dong, "Dynamic performance enhancement method based on improved model reference adaptive system for SPMSM sensorless drives," *IEEE Access*, vol. 9, pp. 135012–135023, 2021.
[29] P. Cortes, J. Rodriguez, C. Silva, and A. Flores, "Delay compensation in model predictive current control of a three-phase inverter," *IEEE Trans. Ind. Electron.*, vol. 59, no. 2, pp. 1323–1325, Feb. 2012.

PENG WANG was born in Jiangsu, China. He received the B.Eng. and M.Sc. degrees in electrical engineering, in 2014 and 2017, respectively. He is currently pursuing the Ph.D. degree with the National Engineering Laboratory for Electric Vehicles, School of Mechanical Engineering, Beijing Institute of Technology. His research interests include synchronous motor drives and multi-phase motor drives.

XIN YUAN (Member, IEEE) received the B.S. and M.S. degrees, in 2013 and 2016, respectively, and the Ph.D. degree in electrical engineering from the Beijing Institute of Technology, Beijing, China, in 2020.

He was a Research Associate at the PEMC Group, University of Nottingham, U.K., from January 2019 to January 2020. He is currently a Research Fellow with the School of Electrical and Electronic Engineering, Nanyang Technological University, Singapore. His research interests include AC motor drives, power converters, multi-phase motor drives, and fault-tolerant strategy of motor.

CHENGNING ZHANG received the M.E. degree in control theory and control engineering and the Ph.D. degree in vehicle engineering from the Beijing Institute of Technology, Beijing, China, in 1989 and 2001, respectively.

He is currently a Professor and the Vice Director of the National Engineering Laboratory for Electric Vehicles, Beijing Institute of Technology. His research interests include electric vehicles, vehicular electric motor drive systems, battery management systems, and chargers.